catalysts

MDPI

Article

Atomic-Level Dispersion of Bismuth over Co_3O_4 Nanocrystals—Outstanding Promotional Effect in Catalytic DeN_2O

Sylwia Wójcik [1], Thomas Thersleff [2,*], Klaudia Gębska [1], Gabriela Grzybek [1] and Andrzej Kotarba [1,*]

[1] Faculty of Chemistry, Jagiellonian University, Gronostajowa 2, 30-387 Krakow, Poland; sylwia.gudyka@doctoral.uj.edu.pl (S.W.); klaudia.gebska18@gmail.com (K.G.); g.grzybek@uj.edu.pl (G.G.)

[2] Department of Materials and Environmental Chemistry, Stockholm University, Svante Arrhenius 16C, 114 18 Stockholm, Sweden

* Correspondence: thomas.thersleff@mmk.su.se (T.T.); ak@uj.edu.pl (A.K.); Tel.: +46-721-675-676 (T.T.); +48-686-25-09 (A.K.)

Received: 4 March 2020; Accepted: 21 March 2020; Published: 22 March 2020

Abstract: A series of cobalt spinel catalysts doped with bismuth in a broad range of 0–15.4 wt % was prepared by the co-precipitation method. The catalysts were thoroughly characterized by several physicochemical methods (X-ray fluorescence spectroscopy (XRF), X-ray diffraction (XRD), Raman spectroscopy (μRS), X-ray photoelectron spectroscopy (XPS), nitrogen adsorption analyzed with Brunaer-Emmett-Teller theory (N_2-BET), work function measurements (WF)), as well as aberration-corrected scanning transmission electron microscopy (STEM) coupled with energy-dispersive X-ray spectroscopy (EDX) and electron energy-loss spectroscopy (EELS). The optimal bismuth promoter content was found to be 6.6 wt %, which remarkably enhanced the performance of the cobalt spinel catalyst, shifting the N_2O decomposition (deN_2O) temperature window ($T_{50\%}$) down from approximately 400 °C (for Co_3O_4) to 240 °C (for the 6.6 wt % Bi-Co_3O_4 catalyst). The high-resolution STEM images revealed that the high activity of the 6.6 wt % Bi-Co_3O_4 catalyst can be associated with an even, atomic-level dispersion (3.5 at. nm^{-2}) of bismuth over the surface of cobalt spinel nanocrystals. The improvement in catalytic activity was accompanied by an observed increase in the work function. We concluded that Bi promoted mostly the oxygen recombination step of a deN_2O reaction, thus demonstrating for the first time the key role of the atomic-level dispersion of a surface promoter in deN_2O reactions.

Keywords: N_2O decomposition; Co_3O_4 nanocrystals; atomic-level dispersion of a promoter

1. Introduction

One of the most important challenges facing society today is the environmental pollution crisis. That is why extensive research is carried out nowadays on various strategies for the reduction of air pollutions emission [1]. In a large group of harmful substances, of which the presence in the atmosphere has a direct negative impact on the natural environment, and greenhouse gases such as CO_2, CH_4, N_2O, O_3, $H_2O_{(g)}$, and freons are drawing special attention [2]. Since the United Nations has set emission limits, both academia and industry focus on the development of the most efficient solutions to reduce anthropogenic emissions into the atmosphere. One of the most hazardous greenhouse gases is nitrous oxide. Due to its long lifetime, estimated for 150–180 years, N_2O can be considered a permanent atmosphere pollutant with a concentration at a level of 3×10^{-5} vol. % [3]. Moreover, the strength of its negative impact is estimated to be more than 260 times higher than that of CO_2 [4]. Although the total anthropogenic emission of nitrous oxide is dominated by agriculture (accounting

for 75%), we are still able to reduce the rest of the global man-made N_2O emission, caused mainly by transportation, stationary combustion (power plants), and the chemical industry [5]. Besides the negative effects in the atmosphere, nitrous oxide is an important chemical reactant in the market with increasing demand. Particularly, N_2O has applications in several industrial branches, such as automotive, electronics, food and beverages, and medical fields. Due to the wide usage of N_2O as an analgesic and anesthetic agent, currently, the medical industry highly contributes up to 90% [6] of the consumption of the produced N_2O in such countries as Denmark, Iceland, Norway, Sweden, Canada, the U.S., and New Zealand [7]. As a consequence, hospital ventilation systems constitute a significant source of greenhouse gas emissions [8].

Many of oxide phases have been tested for the catalytic decomposition of nitrous oxide (deN_2O) [9,10]. Based on the literature reports, among the transition metal oxide catalysts, the cobalt spinel (Co_3O_4) has been recognized as the most active phase in the deN_2O [11,12]. Extensive research on the cobalt spinel revealed many possible modifications leading to the improvement of its catalytic performance. As recently reported in [13], the spinel morphology can be modified to expose the most desired (100) facets by adjusting the synthesis parameters. Several doping strategies were applied, and these were classified following the localizations of promoters: surface (Na, K, Cs, Ba, and Sr) and bulk (Mg, Al, Zn, and Ni) [14]. Finally, the role of the spinel–promoter interface was pointed out, which had positive (CeO_2) [15] and negative (γ-Al_2O_3) [16] effects.

Among several investigated dopants, alkali promoters at catalyst surfaces improving the electrodonor properties of cobalt spinel were found to be the most effective in the deN_2O. However, it was also reported that alkali promoters at catalyst surfaces are mobile and volatile, which may often cause their loss via thermal desorption at the process conditions (400–600 °C) [17]. The ionic radius of bismuth is comparable with potassium and sodium, and according to Vegard's law, Bi cannot substitute cobalt in spinel structures [18]. Therefore, we decided to explore the possibility of employing the Bi additive as a surface promoter of Co_3O_4 catalysts. We placed particular emphasis on the doping level, localization, and dispersion of bismuth. The catalysts were thoroughly characterized in terms of changes in morphology (high-resolution TEM), electronic properties (work function measurements (WF)), and surface composition (electron energy-loss spectroscopy (EELS), energy-dispersive X-ray spectroscopy (EDX), and X-ray photoelectron spectroscopy (XPS) upon the bismuth doping. As a result, the bismuth mechanistic role in the catalytic deN_2O can be elucidated.

2. Results and Discussion

2.1. Catalytic Activity and Work Function Measurements

The series of the cobalt spinel-based catalysts doped with bismuth in a range of 0–15.4 wt % was screened in a catalytic deN_2O reaction in a flow of model feed (5% N_2O/He). The obtained results of deN_2O tests are summarized in Figure 1, where the temperature of 50% N_2O conversion (pink points) was used as a descriptor of the catalytic activity. In Figure 1, a nonmonotonic relationship between the catalytic activity ($T_{50\%}$) of the doped catalyst and the concentration of the bismuth dopant (C_{Bi}) can be observed. The highest catalytic activity (minimal $T_{50\%}$ value of 240 ± 5 °C) was observed for a bismuth doping level of 6.6 wt %. The promotional effect of bismuth was spectacular, in comparison to previously reported studies on several additives to Co_3O_4 for stimulating its activity in the deN_2O. Whereas the reported decrease of $T_{50\%}$ for typical promoters with the optimized concentrations was 70°C for zinc (11 wt %), 85 °C for cerium (11 wt %), and 115 °C for potassium (0.4 wt %) [14], an addition of bismuth (6.6 wt %) shifted a temperature window of the deN_2O reaction by more than 160 °C. Since the promotional effect is usually achieved for a narrow range of additive concentration, the optimum level for each individual promoter had to be found. Thus, after passing the optimal level of doping, the spinel activity was decreased—$T_{50\%}$ increased by 50 °C for the 15.4 wt % Bi-Co_3O_4 catalyst (Figure 1).

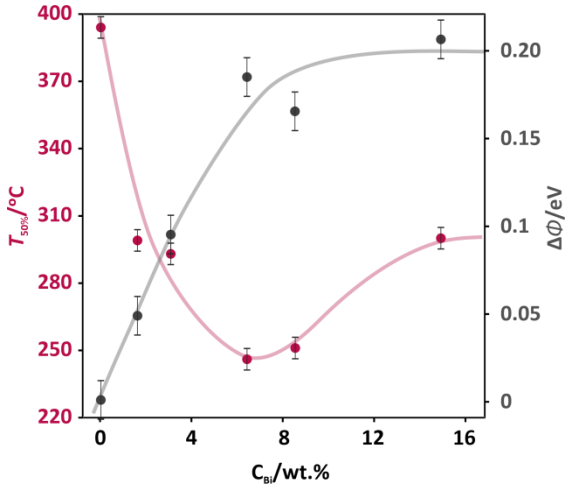

Figure 1. The catalytic activity expressed as the temperature of 50% N_2O conversion ($T_{50\%}$) and work function change ($\Delta\Phi$) as a function of the Bi promoter concentration (C_{Bi}) for the Co_3O_4-based catalysts.

For the cobalt-spinel-based catalysts, the work function was used as a guiding parameter for the optimization of the promoter content. The optimal level of zinc was associated with the decrease of work function (WF) by 0.44 eV, while for a more effective potassium promoter the change in work function ($\Delta\Phi$) was 0.64 eV [14]. The changes in work function ($\Delta\Phi$) versus the bismuth concentration (C_{Bi}) for the investigated catalysts are presented in Figure 1 (grey points). In contrast to previously reported promotional effects related to the work function decrease, the addition of bismuth to the cobalt spinel catalyst caused the increase in the work function in the whole range of Bi concentration. Up to the 6.6 wt % bismuth content, the work function sharply increased by 0.18 eV, reaching a plateau for higher Bi concentrations (8.2 and 15.4 wt %). The increase in WF upon the bismuth addition revealed a different nature of the promotional effect in the deN_2O in comparison to previous reports, where the decrease in WF was found to be beneficial. In order to understand this difference, the mechanism of the deN_2O should be evoked [19]. The deN_2O reaction occurred in two main demanding steps: 1) the activation of a N_2O molecule by an electron transfer from the catalytic surface to the N_2O molecule, resulting in the release of N_2 and surface oxygen ($N_2O_{(g)} + e^- \rightarrow N_{2(g)} + O^-_{surf}$); 2) the recombination of oxygen and its desorption with the transfer of an electron to the catalyst surface ($2O^-_{surf} \rightarrow O_{2(g)} + 2e^-$). The high energetic barrier of these deN_2O steps was calculated by DFT (density functional theory) and reported in [20]. Both the activation of the N_2O molecule and the oxygen recombination required overcoming barriers of 20.1 and 23.4 kcal mol^{-1}, respectively.

The increase of the work function upon the bismuth addition suggested that the dopant facilitated the oxygen recombination step. This may explain why the effect of bismuth on the deN_2O was so large ($\Delta T_{50\%} \approx 160$ °C). A similar effect was observed for the promotion of cobalt spinel by lead in the deN_2O reactions [21], where the optimal dopant concentration was related to the maximum WF of the spinel surface.

In order to exclude the effect of surface area changes of the catalysts, occurring upon the Bi addition (Table 1), the results of deN_2O activity were also presented in the form of reaction rates expressed in μmol m^{-2} s^{-1} (see Figure 2). All the functions of the reaction rates for 250, 300, 350, and 400 °C versus the concentration of Bi (Figure 2) exhibited nonmonotonous profiles, where the maxima corresponded to the lowest promotional level (1.7 wt % Bi). For higher Bi concentrations (3.4, 6.6, and 8.2 wt %), significant decreases in rate can be observed. Such dependences revealed that the most prominent electronic effect of doping was observed for the lowest Bi concentration. A further improvement of the deN_2O activity (Figure 1, pink curve) was related to the increase of the specific surface area (SSA) (Table 1).

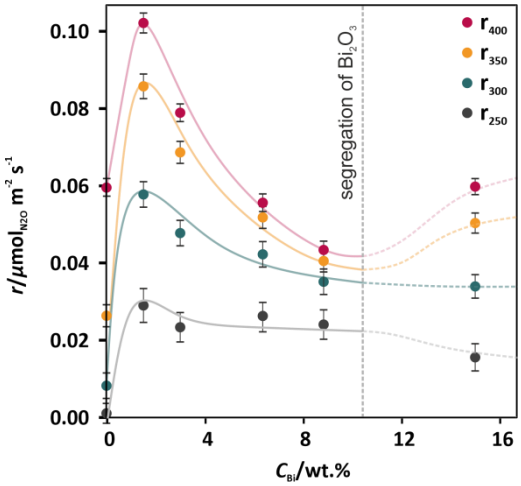

Figure 2. Rates of the catalytic N_2O decomposition for the undoped Co_3O_4 catalyst and the Co_3O_4 catalysts doped with 1.7–15.4 wt % of Bi (the lines illustrate graphically the observed trends).

Table 1. Characterization of the undoped and Bi-doped spinel-based catalysts: nominal and experimental (X-ray fluorescence spectroscopy (XRF)) concentrations of bismuth, surface concentration of bismuth (X-ray photoelectron spectroscopy (XPS)), values of specific surface area (SSA) and Co_3O_4 crystals size determined by the Williamson–Hall (W–H) method, applied to the results of the X-ray diffraction (XRD) measurements.

Sample	Nominal Concentration of Bi (wt %)	Experimental Concentration of Bi (wt %)	Surface Concentration of Bi (at. %)	SSA (m^2 g^{-1})	Co_3O_4 Crystals Size by the W–H Method (nm)
1	0	0	0	33.1	56
2	1.7	1.7 ± 0.3	1.8	32.3	47
3	3.4	3.4 ± 0.2	2.1	43.0	38
4	6.6	6.6 ± 0.4	3.7	57.7	24
5	8.2	9.0 ± 0.3	-	80.8	14
6	15.4	14.6 ± 0.6	3.7	53.7	28

In order to understand the complex nature of the bismuth promotional effect, a series of catalysts was analyzed in terms of phase and surface composition and morphological changes, which are discussed in the next sections.

2.2. Physicochemical Characterization

The desired concentrations of the bismuth promoter, verified by means of X-ray fluorescence spectroscopy (XRF) measurements, were successfully achieved (Table 1, columns 2 and 3) for the whole range of bismuth concentration (1.7–15.4 wt %). Therefore, the catalysts were labeled in the paper using nominal concentrations expressed in wt %.

The results of BET measurements (see Table 1, column 5) indicated a dramatic increase in SSA, even by more than 2.5 times for 8.2 wt % of Bi. This systematic growth was proportional to the concentration of the added Bi, with the exception of the 15.4 wt % Bi-Co_3O_4 catalyst. The decline that was noticed may be the result of the segregation of the bismuth oxide phase. Thus, a spectroscopic phase composition analysis was carried out. The Raman spectra in Figure 3 showed five peaks at 194, 479, 518, 616, and 688 cm^{-1}, which are characteristic of the cobalt spinel phase, and corresponded to the following vibrational modes F_{2g}, E_g, F_{2g}, F_{2g}, and A_{1g}, respectively. There were no significant shifts in the positions of the peaks between different catalysts. However, besides features characteristic of the cobalt spinel, additional signals for the overdoped 15.4 wt % Bi-Co_3O_4 catalyst were registered (see Figure 3, grey brackets on a pink curve). The low-intensity bands in the upper part of the spectrum

located in the range of 105–130 cm^{-1} and at 315 cm^{-1} were characteristic of the bismuth–oxygen vibrations in the BiO_6 unit of the Bi_2O_3 phase [22]. The addition of the dopant with the 15.4 wt % concentration caused the segregation of the bismuth oxide phase, observed also in the decrease of SSA (Table 1). The overdoping of the spinel catalyst probably led to the overlaying of the cobalt active centers by Bi_2O_3 and finally to the partial deactivation of the catalyst.

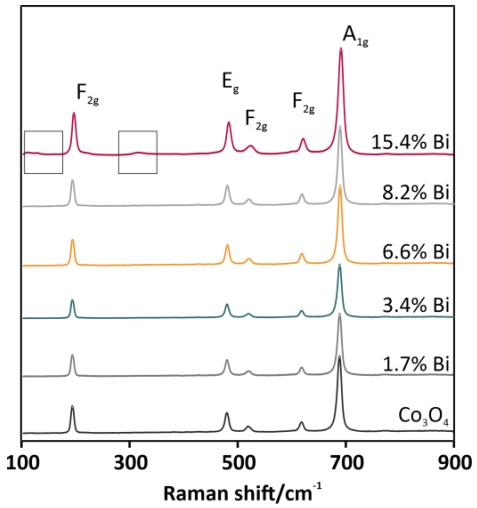

Figure 3. Raman spectra for Co_3O_4-based catalysts doped with bismuth in a range of 0–15.4 wt %.

The surface compositions of the selected catalysts (undoped Co_3O_4 and spinel doped with 1.7, 3.4, 6.6, and 15.4 wt % of Bi) were investigated by means of X-ray photoelectron spectroscopy (XPS). Spectral regions characteristic of cobalt and bismuth are depicted in Figure 4. The analysis of the spectra in the energy range between 750 and 810 eV revealed the presence of several overlapped peaks characteristic of the Co^{2+} (the binding energy level of Co $2p_{3/2}$: 780.2 eV; the binding energy level of Co $2p_{1/2}$: 796.0 eV) and Co^{3+} (the binding energy level of Co $2p_{3/2}$: 779.0 eV; the binding energy level of Co $2p_{3/1}$: 794.1 eV) cations of the cobalt spinel lattice [23]. The spectra also contained features characteristic of Co_3O_4 satellite structures, which were localized around energies of 783.5–789.5 and 804.1 eV. The constant peaks separation (15.3 eV) and the stable positions of the peaks noticed for all collected spectra confirmed the presence of a cobalt spinel structure, remaining intact even upon the bismuth doping. In the spectral region between 155 and 170 eV (Figure 4), two symmetric peaks located at 158.4 and 163.8 eV can be observed. Based on the position of the peaks and their separation distance (5.4 eV), the oxidation state of bismuth in the oxide phase can be determined as Bi^{3+} [24]. Visible changes in the growing intensities of the 4f peaks originated from bismuth were consistent with the increasing content of the dopant in the catalysts. The XPS analysis allowed for the determination of the surface concentration of the bismuth dopant, which are summarized in Table 1 (column 4). The systematic increase of the bismuth surface coverage can be observed in the series of the catalysts. However, the values of the dopant surface concentration determined by the XPS measurements were definitely higher than the concentrations of Bi determined in the XRF measurements. We therefore argued that the Bi promoter was preferentially localized on the surface of the catalysts.

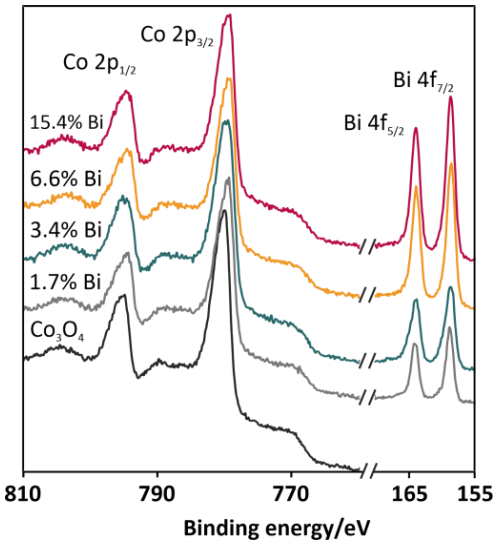

Figure 4. XPS spectra for the selected catalysts (undoped Co_3O_4 and Co_3O_4 doped with 1.7, 3.4, 6.6, and 15.4 wt % of Bi) with particular emphasis on the Co 2p and Bi 4f binding energies.

2.3. High-Resolution Microscopy and Spectroscopy

The morphology of a reference cobalt spinel (Co_3O_4) and a catalyst doped with bismuth at the optimal concentration (6.6 wt % Bi-Co_3O_4) was investigated by scanning transmission electron microscopy (STEM). In addition, the fine structures of cobalt and oxygen were studied by EELS, and elemental composition was confirmed by EDX. The use of a high-angle annular dark-field (HAADF) detector for the STEM images yielded a strong Z-contrast, and the STEM images are shown in Figure 5. The general analysis of the morphology of the catalysts indicated a rombicubooctahedral shape of cobalt spinel crystals (Figure 5A_1,A_2) with sharp edges and sizes between 20 and 50 nm (Figure 5A_3). These features are characteristic of a pure Co_3O_4 phase obtained via a precipitation method [21]. In comparison to the bare spinel phase, the morphology of the catalyst doped with bismuth (see Figure 5B_1,B_2) was significantly different. Whereas the shapes of crystals were comparable and preserved, a remarkable decrease in grain size can be observed. The crystal size of the 6.6 wt % Bi-Co_3O_4 catalyst (Figure 5B_3) was in a range of 5–20 nm with a sharp maximum distribution at 12 nm. The remarkably smaller size of the spinel grains was consistent with the increase in SSA observed upon the bismuth addition (Table 1, column 5), as well as with the crystal size determined by the Williamson–Hall method (Table 1, column 6).

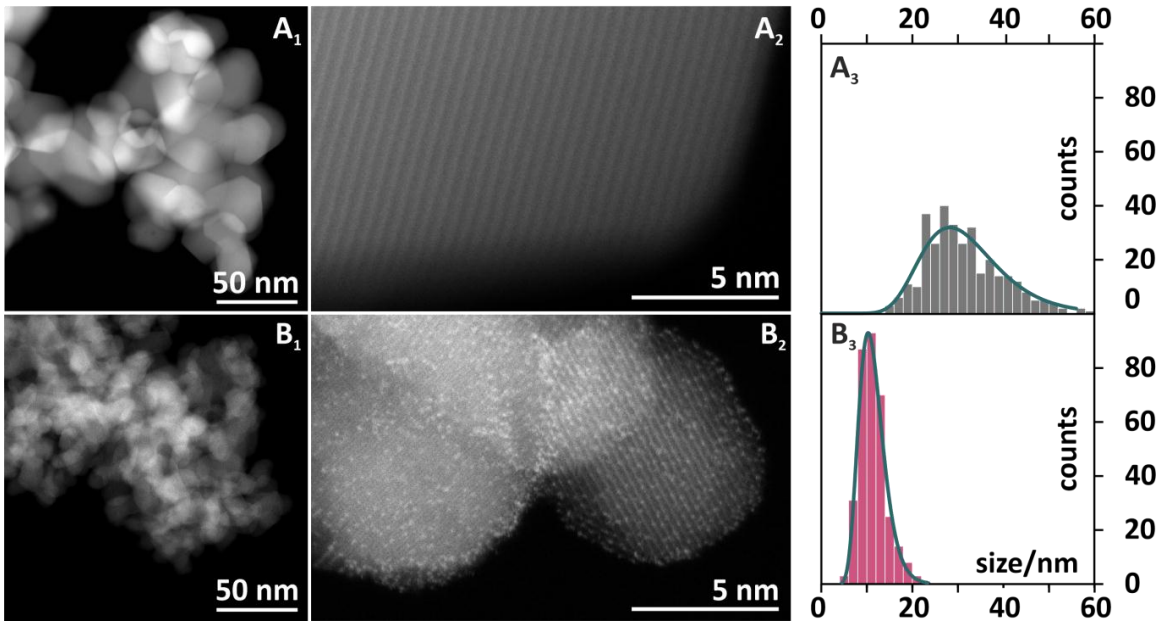

Figure 5. High-angle annular dark-field scanning transmission electron microscopy (HAADF-STEM) images of the Co_3O_4 (**A1**, **A2**) and 6.6 wt % Bi-Co_3O_4 (**B1**, **B2**) catalysts with the distributions of nanoparticles size (**A3** and **B3**, respectively). Histograms are based on n = 350 measurements of individual crystallites.

In the high-resolution image (Figure 5B_2) of the 6.6 wt % Bi-Co_3O_4 catalyst, small bright spots evenly dispersed over the Co_3O_4 crystallites were observed. The use of the HAADF detector in STEM mode preferentially collected electrons that underwent Rutherford scattering events, meaning that the intensity in the image was roughly proportional to the local average atomic mass [25]. The very large difference in atomic masses between cobalt (Z_{Co} = 27) and bismuth (Z_{Bi} = 82) allowed for a clear distinction to be made between bismuth and cobalt, with bismuth-containing regions yielding a much brighter intensity in these images. These regions manifested themselves as bright spots with a diameter around 1–1.5 Å (Figure 5B_2), consistent with their interpretation as individual Bi^{3+} cations or few-atom clusters distributed over the cobalt spinel surface. A thorough analysis of the lattice spacing of the Co_3O_4 particles from a series of HAADF images is summarized in Table 2. Experimentally measured distances for pure spinel nanocrystals slightly differed from the calculated values, because the theoretical numbers described exactly the features of bulk materials. The distances measured for the bare and doped spinel catalysts were similar and varied only within the experimental errors. This suggested that bigger Bi^{3+} (radius of Bi^{3+}_{Oh} = 1.17 Å) [26] atoms did not substitute the cobalt spinel cations (the radii of Co^{2+}_{Td} and Co^{3+}_{Oh} were 0.72 and 0.75 Å, respectively) [26] in the bulk structure of the active phase, thereby confirming the decoration of the Co_3O_4 crystallites by the promoter. We, moreover, noted that bismuth was preferentially localized on the spinel facets. Consequently, the presence of the promoter may result in the termination of the growth of the Co_3O_4 crystallites during its synthesis. This may be one explanation for the significant decrease of the spinel crystal size upon the Bi addition (Figure 5A_3,B_3), manifested also as the increase in SSA (Table 1).

Table 2. Comparison of the theoretical and experimental distances of the selected lattice planes ((111), (200), (210), (220), (310), and (311)) in the bare (Co_3O_4) and doped (6.6 wt % Bi-Co_3O_4) catalytic nanocrystals.

d-Spacing Plane	Theoretical Distances for Bulk Spinel (Å)	* Measured Distances for Co_3O_4 (Å)	* Measured Distances for 0.08Bi-Co_3O_4 (Å)
111	4.67	4.72 ± 0.04	4.71 ± 0.05
200	4.04	4.09 ± 0.02	4.06 ± 0.01
210	3.62	3.58 ± 0.01	3.65 ± 0.01
220	2.86	2.88 ± 0.01	2.89 ± 0.01
310	2.56	2.53 ± 0.01	2.54 ± 0.01
311	2.44	2.45 ± 0.01	2.45 ± 0.02

* Each value is an average of at least 30 crystals measurements.

The EDX analysis (Figure 6, bottom spectra) of the Co_3O_4 and 6.6 wt % Bi-Co_3O_4 catalysts confirmed that the Co:O stoichiometry was similar to the ratio in the cobalt spinel [27]. In addition, the total concentration of bismuth in the promoted catalyst was determined to be 7.4 wt %, consistent with the XRF results. The spectra of the EELS analysis after the background subtraction and deconvolution with the use of the zero-loss peak are shown in the upper part of Figure 6. The spectra of both catalysts showed three overlapping peaks in the range of 530–550 eV, which matched well to the lattice oxygen of the cobalt spinel [28]. However, a more detailed inspection revealed a slight difference in the ratios of the first and second O–K oxygen peaks (see the shadowed insert in Figure 6). As previously shown by Zhang [28], this decrease in the intensity of the O–K prepeak observed for Bi-Co_3O_4 was associated with a reduction in the number of Co–O bonds, leading to a more metallic character. In our system, we interpreted this as the gentle weakening of the Co–O bonding caused by the presence of bismuth cations on the catalyst surface. Such surface promotion resulted in the facilitation of the oxygen recombination step in deN_2O. In the further part of the EELS spectra (Figure 6, top part) two Co white lines (L_3 and L_2) located at 780–800 eV with a separation of 15.5 eV were observed. The similar shape of the fine structure on the Co ionization edge between these two spectra demonstrated that the structure of the cobalt spinel remained intact. Despite this, the ratios of intensities between the Co L_3 and L_2 edges (the white line ratio) for the pure and doped catalysts were slightly different (2.35 and 2.70, respectively). While both values were close to the theoretical value of 2.42 for the pure cobalt spinel [29], this difference hinted at local modifications to the Co oxidation state due to the presence of the Bi promoter. This will be studied in further detail in future experiments.

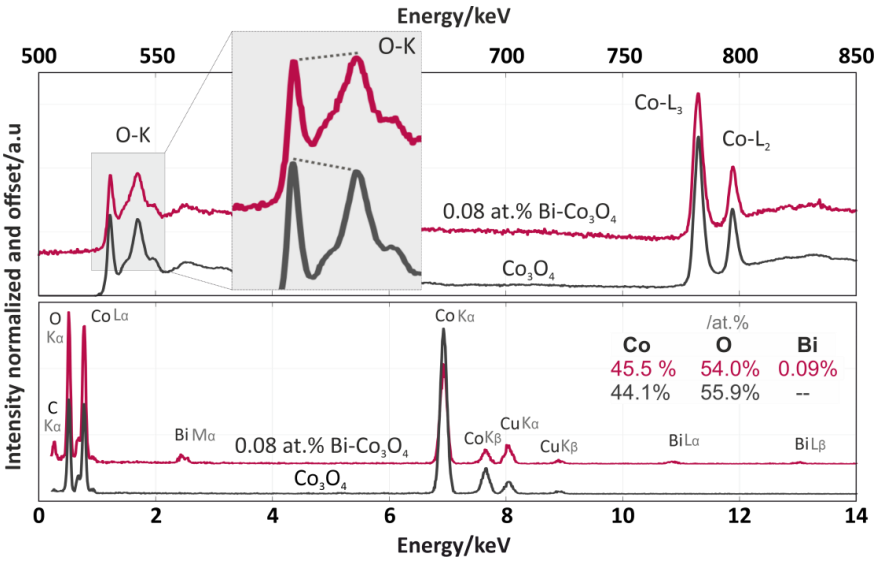

Figure 6. Electron energy-loss spectroscopy (EELS) (upper part) and energy-dispersive X-ray spectroscopy (EDX) (bottom part) spectra of the Co_3O_4 (grey) and 6.6 wt % Bi-Co_3O_4 (pink) catalysts.

The obtained results clearly revealed the double role of the bismuth promoter. On the one hand, the dopant influenced the electronic factor of the cobalt spinel catalyst demonstrated by the WF increase and resulted in the facilitation of the second limiting step in the deN_2O. On the other hand, adding a higher amount of bismuth influenced the morphology of the cobalt spinel phase, causing significant increases of the spinel crystal size (XRD data analyzed by the Williamson–Hall method as well as TEM observations) and the SSA (Table 1), leading to an increase in accessible active centers. The maximal promotional effect was obtained for the optimal bismuth addition, when the tuning of electrodonor properties was accompanied by the increase in SSA. The precise adjustment of the dopant concentration was particularly important, since the active sites were related to the surface of an octahedral Co complex (reported in [11]); a higher concentration of bismuth led to the active sites blocking.

As revealed by HR-TEM (Figure 5), the presence of an even atomic-level surface dispersion of the dopant resulted in an increase in the work function of the catalytic surface (Figure 1). This facilitated the oxygen recombination step in the deN_2O, thereby revealing the mechanistic role of the Bi promoter. The surface localization of bismuth over the spinel crystals facets provided a potential explanation for the small size of the active-phase nanograins (Figure 5A_3,B_3). This led to a doubling of the SSA and an increase in catalytically active cobalt sites. The strong promotional effect of bismuth persisted even after long-term laboratory stability tests carried out by overheating the structured 6.6 wt % Bi-Co_3O_4-based catalyst in the flow of reaction gases at 600 °C for 20 h (Appendix A). The practical importance of the obtained results consisted in shifting down the temperature window of the deN_2O process from $T_{50\%} \approx 400$ °C (for Co_3O_4) to $T_{50\%} \approx 240$ °C (for 6.6 wt % Bi-Co_3O_4), which is essential for potential applications of cobalt-spinel-based catalysts in a low-temperature regime [21,30].

3. Materials and Methods

3.1. Synthesis of Co_3O_4-Based Catalysts

A series of cobalt-spinel-based catalysts doped with bismuth in a concentration range (0–15.4 wt %) was obtained via a co-precipitation method. The substrates of cobalt nitrate(V) hexahydrate and bismuth(III) nitrate pentahydrate were dissolved in an aqueous solution of nitric acid (2 mol L^{-1}) in order to obtain 1 M concentration of cations. Then, the prepared mixture was precipitated by a solution (1 M) of ammonia carbonate(IV) (POCH), until the pH value of the mixture was 8.2. In the next step, the sediment was filtered on a Buckner funnel and washed, until the pH became neutral. The precipitate was dried at 80 °C for 12 h) and calcined at 500 °C for 4 h in the air conditions. The reference sample of the undoped cobalt spinel was obtained with the use of the same procedure but without the addition of bismuth salt.

3.2. DeN_2O Tests and Work Function Measurements

Screening of the catalytic activity in the deN_2O was performed in the temperature-programmed surface reaction (TPSR) mode. The sieve fraction (0.2–0.3 mm) of each powdered catalyst was placed on a sintered glass in a quartz flow reactor. The activity of the catalysts was investigated in a flow of model gases (50,000 ppm of N_2O in He) with the prior sample cleaning done by the heating, until the temperature was 500 °C in the flow of reaction gases. Taking into account the mass of the catalysts (0.3 g) and the flow rate (30 mL s^{-1}), the gas space velocity in the test was estimated to be 7000 h^{-1}. The concentration levels of individual gas-phase components (m/z = 18 (for H_2O), 28 (for N_2), 32 (for O_2), and 44 (for N_2O)) during the catalytic reaction were continuously measured by means of a quadrupole mass spectrometer RGA200, SRS (Stanford Research Systems, Sunnyvale, CA, USA). To ensure that the reactor operated in the kinetic regime, the catalytic experiments were designed in line with the Eurokin standards [31].

The influence of the bismuth dopant on the electronic properties of the cobalt spinel catalysts was investigated by means of the work function. The series of catalysts was examined by the Kelvin

dynamic condenser method with a KP 6500 probe by McAllister Technical Services (Coeur d'Alene, ID, USA). As a reference electrode in the experiments, a stainless-steel plate with a 3 mm diameter and a work function determined at Φ = 4.3 eV was used. The measurements of the catalyst work function were carried out in the mild conditions of room temperature and atmospheric pressure. The obtained results of $\Delta\Phi$ were the average of 100 points measured with a vibration frequency set at 114 Hz and an amplitude set at 40 of arbitrary units.

3.3. Physicochemical Characterization

The elemental composition of the synthesized samples was verified by means of XRF, with the use of a Thermo Scientific (Waltham, MA, USA) ARL QUANT'X apparatus. Data were collected after calibration into a series of metallic standards. Measurements, calibration, and data analysis were carried out using the UniQuant software.

The SSAs of the obtained catalysts were investigated by the nitrogen absorption–desorption measurements performed at 77 K with the use of a Micromeritics (Norcross, GA, USA) ASAP 2010 instrument. Each catalyst sample was outgassed under vacuum at 623 K for 12 h before the measurements. The obtained data were analyzed accordingly to the method of BET isotherm.

The series of the obtained catalysts was analyzed for the phase composition by means of Raman spectroscopy measurements. For this purpose, a Renishaw (Wotton-under-Edge, UK) InVia spectrometer with a Leica DMLM confocal microscope and a CCD detector was used. Experiments were carried out at room temperature, using a laser with a wavelength of 785 nm. The spectra were registered in a range of 100–900 cm^{-1}. To achieve a high signal-to-noise ratio, 12 subsequent scans were accumulated. Besides the phase composition, the size of the crystals of the active phase was evaluated. Based on the XRD measurements (not included), the spinel crystal size was calculated with the use of the Williamson–Hall method.

The elemental surface compositions of the selected catalysts (bare Co_3O_4 and spinel Co_3O_4 doped with bismuth: 1.7, 3.4, 6.6, 8.2, and 15.4 wt %) were investigated by the XPS method. For the measurements, a Prevac (Rogow, Poland) spectrometer equipped with a hemispherical VG SCIENTA R3000 analyzer was used. The spectra were collected with the use of a monochromatized Al Kα source with an energy E of 1486.6 eV (pass energy of 100 eV) and an electron flood gun (FS40A-PS). For the analysis of the obtained data, the CasaXPS software was used. All spectra were calibrated into the carbon peak C1s at 284.8 eV.

3.4. High-Resolution Microscopy and Spectroscopy

Nanoscale analysis of the morphologies and compositions of the Co_3O_4 and 6.6 wt % Bi-Co_3O_4 catalysts was carried out by aberration-corrected STEM, EELS, and EDX). A Themis Z TEM (FEI, Eindhoven, The Netherlands) operating at 300 kV was corrected up to fifth-order aberrations. This instrument was equipped with a SuperX EDX detector and a Quantum ERS EELS spectrometer (Gatan Inc, (Pleasanton, CA, USA), permitting simultaneous EELS and EDX acquisition. All of the imaging and spectroscopy data were collected in the STEM mode with a convergence semiangle of 19.5 mrad, while the EELS data were collected with a collection angle of 17 mrad. The EELS and EDX spectra for each sample in Figure 6 were the sums of more than 10,000 serially acquired spectra acquired as spectrum images. Plural scattering was removed from the core-loss spectra shown in Figure 6 (upper part) by Fourier-ratio deconvolution using the simultaneously acquired low-loss spectra. Consequently, the spectra in Figure 6 were not strongly influenced by variations in thickness and thus closely resembled the true single scattering distributions of the Co_3O_4 and 6.6 wt % Bi-Co_3O_4 catalysts. TEM grids were prepared via the glow charge method with the use of argon plasma. Additionally, prior to all the experiments, each sample was cleaned under oxygen plasma for approximately 10 seconds to reduce carbon contamination.

4. Conclusions

A series of Co_3O_4-based catalysts doped with bismuth (1.7–15.4 wt %) was synthesized, characterized (XRF, μRS, XPS, WF, and TEM/EDX/EELS) and evaluated for a low-temperature (<450 °C) deN_2O (TPSR). The optimal level of doping was found to be 6.6 wt %, which resulted in a spectacular improvement of the spinel activity ($T_{50\%}$ lowered by 160 °C). The high-resolution STEM images revealed the atomic-level decoration of the spinel crystals surface with the Bi promoter. Such a specific localization of the promoter, hindering the growth of spinel crystals, led to an increase in SSA from 33.1 m^2 g^{-1} for the undoped Co_3O_4 to 57.7 m^2 g^{-1} for the 6.6 wt % Bi-Co_3O_4 catalyst. Besides the morphological changes, we observed that the optimal Bi loading corresponded to the maximal work function of the spinel catalyst. Such a change in electronic properties revealed that the promotion effect consisted in facilitating the oxygen recombination—the most demanding step in the mechanistic pathway of the deN_2O. The single-site promotion was proposed for the first time as an effective strategy for the improvement of cobalt spinel performance in the deN_2O process.

Author Contributions: Conceptualization, A.K.; methodology, T.T. and A.K.; formal analysis, S.W. and T.T.; investigation, S.W., T.T., and K.G.; data curation, S.W. and T.T.; writing of the original draft preparation, S.W.; writing of review and editing, G.G., T.T., and A.K.; visualization, S.W. and T.T.; supervision, A.K.; funding acquisition, S.W. and T.T. All authors have read and agreed to the published version of the manuscript.

Funding: This research was funded by the Polish National Science Center (grant number: 2016/23/N/ST8/01512). S.W. received funding for the preparation of her doctoral dissertation from the Polish National Science Center under the doctoral scholarship funding program (decision number: 2019/32/T/ST4/00185). T.T. acknowledges funding from the Swedish Research Council (project nr. 2016-05113).

Acknowledgments: The research was carried out with the equipment purchased thanks to the financial support of the European Regional Development Fund in the framework of the Polish Innovation Economy Operational Programme (contract no. POIG.02.01.00-12-023/08).

Conflicts of Interest: The authors declare no conflicts of interest.

Appendix A

Long-term and high-temperature stability test:

The most active cobalt-spinel-based catalyst, 6.6 wt % Bi-Co_3O_4 catalyst, was further deposited over the cordierite monolith via a standard impregnation method (see details in a recent paper [21]). The structured catalyst, containing 10 wt % of bismuth promoted a spinel active phase, was aged in high-temperature conditions at 600 °C for 20 h in a flow of reaction gases (5% N_2O/He, flow rate: 30 mL/min). The stability of the promotional effect of bismuth was investigated by the comparison of the N_2O conversion levels at 400 °C (X_{400}) before and after the aging of the catalyst. The N_2O conversion during the aging stage (600 °C) reached and kept the maximum X_{600} value of approximately 100%. The conversion levels of N_2O monitored at 400 °C (X_{400}) before and after the long-term aging of the catalyst were the same and equal to approximately 85%. This result confirmed the stability of the deposited 6.6 wt %—active phase and the persistence of the strong promotional effect of the bismuth dopant, even in high-temperature conditions.

References

1. *Reducing Global Health Risk. Through Mitigation of Short-Lived Climate Pollutants Scoping Report for Policymakers*; World Health Organization: Geneva, Switzerland, 2015.
2. *Inventory of Greenhouse Gas Emissions and Sinks: 1990–2016*; Environmental Protection Agency: Washington, DC, USA, 2018.
3. Denisova, K.O.; Ilyin, A.A.; Rumyantsev, R.N.; Ilyin, A.P.; Volkova, A.V. Nitrous Oxide: Production, Application, and Protection of the Environment. *Russ. J. Gen. Chem.* **2019**, *89*, 46–54. [CrossRef]
4. Global Warming Potential Values. Available online: https://www.ghgprotocol.org/sites/default/files/ghgp/Global-Warming-Potential-Values%20%28Feb%2016%202016%29_1.pdf (accessed on 22 March 2020).

5. *Drawing Down N2O To Protect Climate and the Ozone Layer A UNEP Synthesis Report*; United Nations Environment Programme (UNEP): Nairobi, Kenya, 2013.
6. Nitrous Oxide Market Size & Share|Global Industry Report, 2018–2025. Available online: https://www.grandviewresearch.com/industry-analysis/nitrous-oxide-market (accessed on 4 March 2020).
7. Ek, M.; Tjus, K. *Destruction of Medical N2O in Sweden. Greenhouse Gases—Capturing, Utilization and Reduction*; InTech: London, UK, 2012.
8. Husum, B.; Stenqvist, O.; Alahuhta, S.; Sigurdsson, G.H.; Dale, O. Current use of nitrous oxide in public hospitals in Scandinavian countries. *Acta Anaesthesiol. Scand.* **2013**, *57*, 1131–1137. [CrossRef] [PubMed]
9. Konsolakis, M. Recent Advances on Nitrous Oxide (N_2O) Decomposition over Non-Noble-Metal Oxide Catalysts: Catalytic Performance, Mechanistic Considerations, and Surface Chemistry Aspects. *ACS Catal.* **2015**, *5*, 6397–6421. [CrossRef]
10. Obalová, L.; Pacultová, K.; Balabánová, J.; Jirátová, K.; Bastl, Z.; Valášková, M.; Lacný, Z.; Kovanda, F. Effect of Mn/Al ratio in Co-Mn-Al mixed oxide catalysts prepared from hydrotalcite-like precursors on catalytic decomposition of N_2O. *Catal. Today* **2007**, *119*, 233–238. [CrossRef]
11. Kaczmarczyk, J.; Zasada, F.; Janas, J.; Indyka, P.; Piskorz, W.; Kotarba, A.; Sojka, Z. Thermodynamic Stability, Redox Properties, and Reactivity of Mn_3O_4, Fe_3O_4, and Co_3O_4 Model Catalysts for N_2O Decomposition: Resolving the Origins of Steady Turnover. *ACS Catal.* **2016**, *6*, 1235–1246. [CrossRef]
12. Abu-Zied, B.M.; Asiri, A.M. The role of alkali promoters in enhancing the direct N_2O decomposition reactivity over NiO catalysts. *Cuihua Xuebao/Chin. J. Catal.* **2015**, *36*, 1837–1845. [CrossRef]
13. Gudyka, S.; Grzybek, G.; Gryboś, J.; Indyka, P.; Leszczyński, B.; Kotarba, A.; Sojka, Z. Enhancing the deN_2O activity of the supported Co_3O_4|α-Al_2O_3 catalyst by glycerol-assisted shape engineering of the active phase at the nanoscale. *Appl. Catal. B Environ.* **2017**, *201*, 339–347. [CrossRef]
14. Wójcik, S.; Grzybek, G.; Stelmachowski, P.; Sojka, Z.; Kotarba, A. Bulk, Surface and Interface Promotion of Co_3O_4 for the Low-Temperature N_2O Decomposition Catalysis. *Catalysts* **2019**, *10*, 41. [CrossRef]
15. Rico-Pérez, V.; Kotarba, A.; Sojka, Z.; Indyka, P.; Guillén-Hurtado, N.; Bueno-López, A.; Grzybek, G.; Gudyka, S.; Stelmachowski, P. Strong dispersion effect of cobalt spinel active phase spread over ceria for catalytic N_2O decomposition: The role of the interface periphery. *Appl. Catal. B Environ.* **2015**, *180*, 622–629.
16. Grzybek, G.; Ciura, K.; Wójcik, S.; Gryboś, J.; Indyka, P.; Inger, M.; Antoniak-Jurak, K.; Kowalik, P.; Kotarba, A.; Sojka, Z. On the selection of the best polymorph of Al_2O_3 carriers for supported cobalt nano-spinel catalysts for N_2O abatement: An interplay between preferable surface spreading and damaging active phase-support interaction. *Catal. Sci. Technol.* **2017**, *7*, 5723–5732. [CrossRef]
17. Grzybek, G.; Wójcik, S.; Legutko, P.; Gryboś, J.; Indyka, P.; Leszczyński, B.; Kotarba, A.; Sojka, Z. Thermal stability and repartition of potassium promoter between the support and active phase in the K-$Co_{2.6}Zn_{0.4}O_4$|α-Al_2O_3catalyst for N_2O decomposition: Crucial role of activation temperature on catalytic performance. *Appl. Catal. B Environ.* **2017**, *205*, 597–604. [CrossRef]
18. Denton, A.R.; Ashcroft, N.W. Vegard's Law. *Phys Rev A* **1991**, *43*, 3161–3164. [CrossRef] [PubMed]
19. Tolman, W.B. Binding and activation of N_2O at transition-metal centers: Recent mechanistic insights. *Angew. Chem. Int. Ed.* **2010**, *49*, 1018–1024. [CrossRef] [PubMed]
20. Piskorz, W.; Zasada, F.; Stelmachowski, P.; Kotarba, A.; Sojka, Z. Decomposition of N_2O over the surface of cobalt spinel: A DFT account of reactivity experiments. *Catal. Today* **2008**, *137*, 418–422. [CrossRef]
21. Wójcik, S.; Indyka, P.; Sojka, Z.; Kotarba, A. Development of structured Co_3O_4-based catalyst for N_2O removal from hospital ventilation systems. *Catal. Today* 2019. [CrossRef]
22. Shang, Z.; Sun, M.; Chang, S.; Che, X.; Cao, X.; Wang, L.; Guo, Y.; Zhan, W.; Guo, Y.; Lu, G. Activity and stability of Co_3O_4-based catalysts for soot oxidation: The enhanced effect of Bi_2O_3 on activation and transfer of oxygen. *Appl. Catal. B Environ.* **2017**, *209*, 33–44. [CrossRef]
23. Lou, Y.; Ma, J.; Cao, X.; Wang, L.; Dai, Q.; Zhao, Z.; Cai, Y.; Zhan, W.; Guo, Y.; Hu, P.; et al. Promoting Effects of In_2O_3 on Co_3O_4 for CO Oxidation: Tuning O_2 Activation and CO Adsorption Strength Simultaneously. *ACS Catal.* **2014**, *4*, 4143–4152. [CrossRef]
24. XPS Interpretation of Bishmuth. Available online: https://xpssimplified.com/elements/bismuth.php (accessed on 4 March 2020).
25. Yamashita, S.; Kikkawa, J.; Yanagisawa, K.; Nagai, T.; Ishizuka, K.; Kimoto, K. Atomic number dependence of Z contrast in scanning transmission electron microscopy. *Sci. Rep.* **2018**, *8*, 1–7. [CrossRef]
26. Shannon Radii. Available online: http://abulafia.mt.ic.ac.uk/shannon/ptable.php (accessed on 4 March 2020).

27. Srinivasa Rao, N.; Srinivasa Rao, L.; Srinivasa Rao, C.; Raghavaiah, B.V.; Ravi Kumar, V.; Brik, M.G.; Veeraiah, N. Influence of valence states and co-ordination of cobalt ions on dielectric properties of $PbOBi_2O_3As_2O_3$:CoO glass system. *Phys. B Condens. Matter* **2012**, *407*, 581–588. [CrossRef]
28. Zhang, Z. Surface effects in the energy loss near edge structure of different cobalt oxides. *Ultramicroscopy* **2007**, *107*, 598–603. [CrossRef]
29. Zhao, Y.; Feltes, T.E.; Regalbuto, J.R.; Meyer, R.J.; Klie, R.F. In situ electron energy loss spectroscopy study of metallic Co and Co oxides. *J. Appl. Phys.* **2010**, *108*, 063704. [CrossRef]
30. Inger, M.; Wilk, M.; Saramok, M.; Grzybek, G.; Grodzka, A.; Stelmachowski, P.; Makowski, W.; Kotarba, A.; Sojka, Z. Cobalt spinel catalyst for N_2O abatement in the pilot plant operation-long-term activity and stability in tail gases. *Ind. Eng. Chem. Res.* **2014**, *53*, 10335–10342. [CrossRef]
31. EUROKIN_fixed-bed_html, EUROKIN spreadsheet on requirements for measurement of intrinsic kinetics in the gas-solid fixed-bed reactor. Available online: https://www.eurokin.org/wp-content/uploads/webtool/EUROKIN_fixed-bed_html.htm (accessed on 22 March 2020).